NeuroImage 234 (2021) 117964

Contents lists available at ScienceDirect

NeuroImage

journal homepage: www.elsevier.com/locate/neuroimage

Focal lesions induce large-scale percolation of sleep-like intracerebral activity in awake humans

S. Russo[a,1], A. Pigorini[a,1], E. Mikulan[a], S. Sarasso[a], A. Rubino[b], F.M. Zauli[a], S. Parmigiani[a], P. d'Orio[b,c], A. Cattani[a,d], S. Francione[b], L. Tassi[b], C.L.A. Bassetti[f], G. Lo Russo[b], L. Nobili[e,i], I. Sartori[b], M. Massimini[a,g,h,*]

[a] Department of Biomedical and Clinical Sciences "L. Sacco", University of Milan, Milan, Italy
[b] "C. Munari" Epilepsy Surgery Centre, Department of Neuroscience, Niguarda Hospital, Milan 20162, Italy
[c] Institute of Neuroscience, CNR, via Volturno 39E, 43125 Parma, Italy
[d] Department of Psychiatry, University of Wisconsin-Madison, Madison, WI, 53719, USA
[e] Child Neuropsychiatry, IRCCS Istituto G. Gaslini, Genova 16147, Italy
[f] Department of Neurology, Inselspital, University of Bern, Switzerland
[g] IRCCS, Fondazione Don Carlo Gnocchi, Milan 20148, Italy
[h] Azrieli Program in Brain, Mind and Consciousness, Canadian Institute for Advanced Research, Toronto, Canada
[i] Department of Neurosciences, Rehabilitation, Ophthalmology, Genetics, Maternal and Child Health (DiNOGMI), University of Genoa, Genoa, Italy

ARTICLE INFO

Keywords:
Bistability
Effective connectivity
Intracranial recording
Radio-frequency thermo-coagulation
Stroke

ABSTRACT

Focal cortical lesions are known to result in large-scale functional alterations involving distant areas; however, little is known about the electrophysiological mechanisms underlying these network effects. Here, we addressed this issue by analysing the short and long distance intracranial effects of controlled structural lesions in humans. The changes in Stereo-Electroencephalographic (SEEG) activity after Radiofrequency-Thermocoagulation (RFTC) recorded in 21 epileptic subjects were assessed with respect to baseline resting wakefulness and sleep activity. In addition, Cortico-Cortical Evoked Potentials (CCEPs) recorded before the lesion were employed to interpret these changes with respect to individual long-range connectivity patterns. We found that small structural ablations lead to the generation and large-scale propagation of sleep-like slow waves within the awake brain. These slow waves match those recorded in the same subjects during sleep, are prevalent in perilesional areas, but can percolate up to distances of 60 mm through specific long-range connections, as predicted by CCEPs. Given the known impact of slow waves on information processing and cortical plasticity, demonstrating their intrusion and percolation within the awake brain add key elements to our understanding of network dysfunction after cortical injuries.

1. Introduction

Focal cortical injuries are thought to disrupt neuronal activity across large-scale networks, extending well beyond the area of neuronal loss (Falcon et al., 2016). The occurrence of functional alterations in brain structures that are not directly affected by structural damage, named 'diaschisis' by Von Monakow (Von Monakov 1969; Feeney and Baron 1986) in 1914, has now become a subject of active empirical investigation (Carrera and Tononi 2014; Fornito et al., 2015; Baldassarre et al., 2016). So far, the neural underpinnings of diaschisis have been mainly studied with PET (Levasseur et al., 1992) and fMRI, showing hypo-perfusion (Yamakami and McIntosh 1991), hypo-metabolism (Carmichael et al., 2004; Vagnozzi et al., 2010) (Carmichael et al., 2004; Vagnozzi et al., 2010), and altered functional connectivity (Price et al., 2001; Carter et al., 2012) extending far beyond the site of injury (Siegel et al., 2016). These neuroimaging patterns of functional network disruption are clinically relevant as they can explain behavioural deficits and their recovery (Saenger et al., 2018), however their neuronal underpinnings are still elusive.

Electrophysiological evidence derived from animal models (Gloor et al., 1977; Leemburg et al., 2018) and non-invasive clinical recordings in stroke and traumatic brain injured subjects report a relative slowing of electroencephalographic (EEG) and magnetoencephalographic (MEG) rhythms that is prominent in areas ipsilateral to the lesion (Nuwer et al., 1987a; Butz et al., 2004), may extend to the contralateral hemisphere (Buchkremer-Ratzmann et al.,

* Corresponding author at: Department of Biomedical and Clinical Sciences "L. Sacco", University of Milan, Milan, Italy.
E-mail address: marcello.massimini@unimi.it (M. Massimini).
[1] These authors equally contributed to the present work.

https://doi.org/10.1016/j.neuroimage.2021.117964
Received 6 November 2020; Received in revised form 15 February 2021; Accepted 8 March 2021
Available online 23 March 2021

1996; Rorden and Karnath 2004), and persist in the chronic phase (Poryazova et al., 2015; Cassidy et al., 2020). Furthermore, recent work employing direct cortical perturbations with transcranial magnetic stimulation (TMS) revealed the occurrence of slow EEG responses in the perilesional area associated with disruption of local information processing (Sarasso et al., 2020) and behavioural impairment (Tscherpel et al., 2020). Overall, these macroscopic recordings suggest the interesting possibility that the intrusion of low frequency neuronal activity in anatomically spared cortical tissue represents an important element of functional network disruption after acquired brain injury.

Testing this hypothesis would require revealing the precise nature of post-lesion electrophysiological alterations with respect to pre-lesion activity, their local spatial extent and, most important, their potential for propagating within large-scale networks. So far, however, such systematic exploration has been hampered by fundamental challenges such as (i) the spurious and variable nature (e.g. ischaemic, haemorrhagic, and traumatic) of accidental brain lesions, (ii) the low spatial resolution of non-invasive electrophysiological recording techniques and (iii) the lack of baseline recordings acquired before the injury within the same subject.

In the present study, we overcome these issues by adopting an approach whereby the effects of controlled lesions are assessed with spatially resolved electrophysiological recordings and compared to prelesional measurements within the same individual. To this end, we contrasted spontaneous rest Stereo-Electroencephalography (SEEG) recorded in 21 subjects both before and after the induction of small focal cortical lesions by SEEG-guided Radiofrequency-Thermocoagulation (RFTC) performed as a therapeutic option for drug-resistant focal epilepsy (Cossu et al., 2015a; Bourdillon et al., 2017; Dimova et al., 2017). Baseline measurements included resting activity during NREM sleep and during wakefulness as well as cortico-cortical evoked potentials elicited by single-pulse electrical stimulation to assess individual patterns of long-range connectivity (Matsumoto et al., 2017; Trebaul et al., 2018). We found that post-lesion intracerebral activity during wakefulness was characterized by slow waves closely matching those recorded during baseline NREM sleep in the same individuals. Crucially, these sleep-like slow waves were prominent in the perilesional areas but could also percolate through a network of connected areas as predicted by individual patterns of long-range effective connectivity.

The present results suggest that the generation of focal sleep-like slow waves and their long-range propagation within the awake brain may represent a key electrophysiological component of diaschisis and, more in general, a crucial element for understanding the functional consequences of focal and multi-focal injury.

2. Materials and methods

2.1. Subjects and implantation procedures

Data were collected during the presurgical evaluation of 21 subjects with a history of drug-resistant, focal epilepsy (Supplementary Table 1). SEEG was indicated when a tailored non-invasive presurgical evaluation failed to clearly define the subject's epileptogenic zone (EZ). Intracerebral recordings were performed to define the cerebral structures involved in the onset and propagation of seizures, based on the results of non-invasive evaluations. The placement of intracerebral electrodes was determined solely by the clinical necessity for searching for EZ (Cossu et al., 2015a; Cardinale et al., 2019). Each subject underwent brain MRI (Achieva 1.5 T, Philips Healthcare) and CT (O-arm 1000 system [Medtronic]) to acquire appropriate sequences for SEEG planning. The investigated hemisphere/s (9 Left; 6 Right; 6 Bilateral), the location and the number of explored sites were determined based on the non-invasive anatomo-electro-clinical assessment. The duration of SEEG investigation was based only on clinical needs. Placement of intracerebral electrodes was performed under general anaesthesia by means of a robotized passive tool-holder (Neuromate, Renishaw Mayfield SA). A variable number of platinum–iridium semi flexible multi-contact intracerebral electrodes, with a diameter of 0.8 mm, a contact length of 2 mm, an inter-contact distance of 1.5 mm and a maximum of 18 contacts per electrode (Microdeep intracerebral electrodes, D08 [Dixi Medical], or Depth Electrodes Range 2069 [Alcis]) were placed and fixed. After implantation, a fine cone-beam CT data set was acquired by using the O-arm and coregistered with the T1-weighted 3D MR image to verify the actual position of the electrodes (Cardinale et al., 2019).

2.2. Localisation of SEEG contacts

The precise localisation of each contact was obtained by employing the SEEGA tool (Narizzano et al., 2017) and checked by trained neurophysiologists. Any contact showing an inaccurate position was correctly placed at the centroid of its corresponding CT artefact. The anatomical area of each contact was extracted from Freesurfer's (Fischl 2012) parcellation using the Desikan/Killiany atlas. The position of each contact was normalised to the MNI152 using the ANTs toolbox after brain extraction (Avants et al., 2011) and plotted on a 3D rendering (Fig. 1A) and on a flatmap (Fig. 2A, Supplementary Fig. 1) using *pycortex* (Gao et al., 2015). The distance between each recording contact and the lesion induced by RFTC was operationalized as the minimum Euclidean distance from the recording site and each RFTC site.

2.3. Data acquisition and single pulse electrical stimulation (SPES)

During invasive diagnostic evaluation, 21 subjects underwent individual investigation with spontaneous activity recordings alone or combined with single pulse electrical stimulation (SPES) during eyes open resting wakefulness. In addition, in 19 of the 21 subjects' spontaneous recordings were collected during sleep before RFTC (sleep recordings were not available for subjects 6 and 13). SEEG signals were recorded using a 192-channel recording system (Nihon-Kohden Neurofax-1200) with a sampling rate of 1000 Hz. SEEG data were recorded and exported in EEG Nihon-Kohden format. Recordings were referenced to a contact located entirely in white matter. Besides recordings of spontaneous activity to detect the origin of the ictal discharge, single pulse electrical stimulation (SPES) was performed to identify eloquent areas and effective networks connected with the epileptogenic zone (Valentín et al., 2002; Keller et al., 2011; Matsumoto et al., 2017). SPES was delivered through each pair of adjacent contacts, with at 3–5 mA current intensity, single pulse of 0.5 ms (biphasic rectangular stimuli of alternating polarity), at 1 Hz frequency, for 15 s. In all subjects, 87.26% of the implanted contacts were stimulated, thus obtaining a total amount of 2864 stimulation sessions (average ± std; 143±21 per subject). Stimulation, recording and data treatment procedures were approved by the local Ethical Committee and in line with GDPR (ID 939–2.12.2013, Milano AREA C Niguarda Hospital, Milan, Italy). All subjects provided written informed consent.

2.4. Radiofrequency Thermocoagulation (RFTC)

Radiofrequency Thermocoagulation (RFTC) is a surgical technique that can be executed without anaesthesia/sedation at the end of SEEG investigation with the aim to reduce the number and intensity of seizures before having to resort to more invasive surgery (Guénot et al., 2004; Cossu et al., 2015a; Scholly et al., 2019). RFTC of each target site is performed between a pair of contiguous contacts pertaining to the same electrode (Fig. 1A) and selected according to one of the criteria defined in Cossu et al. (2015b), that are: (1) intralesional location (see Supplementary Table 1), (2) habitual ictal clinical phenomena induced when electrical stimulations were performed on those contiguous contacts, or (3) the contacts are part of the network involved in the ictal discharge. In all cases, they must be silent at functional mapping (e.g., movement, speech, vision) and distant > 2 mm from vascular structures (Cossu et al.,

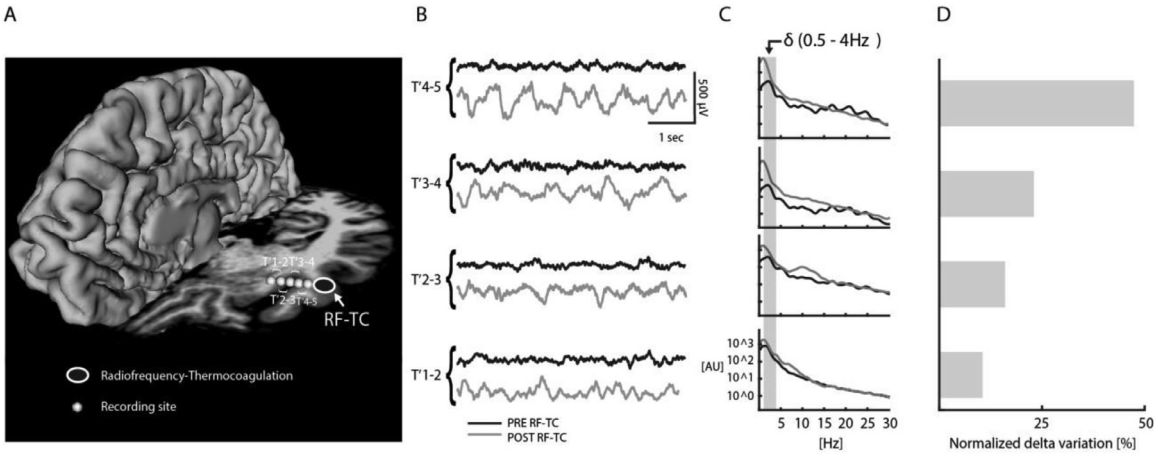

Fig. 1. Recordings from a representative subject. **Panel A**: T1 MRI (axial section of the left hemisphere) and 3D surface reconstruction (of the right hemisphere) from a representative subject showing one RFTC site (black ovoid, T'6–7, left Superior Temporal Gyrus) and four bipolar recording contacts (white points: T'1–2 and T'2–3 in the left Insula,T'3–4 and T'4–5 in left Superior Temporal Gyrus) from the same electrode and progressively distancing from the RFTC. **Panel B**: Spontaneous activity recorded before RFTC (in black) and after RFTC (in grey) from each of the bipolar contact shown in Panel A. **Panel C**: for the same contacts and conditions (same colour-coding), high frequency normalized Power Spectral Density is shown. The grey shaded, vertical band highlights the frequency band selected for delta (0.5 - 4 Hz) quantifications. **Panel D**: for the same representative contacts, percentage delta variation of post-RFTC power with respect to pre-RFTC power is shown.

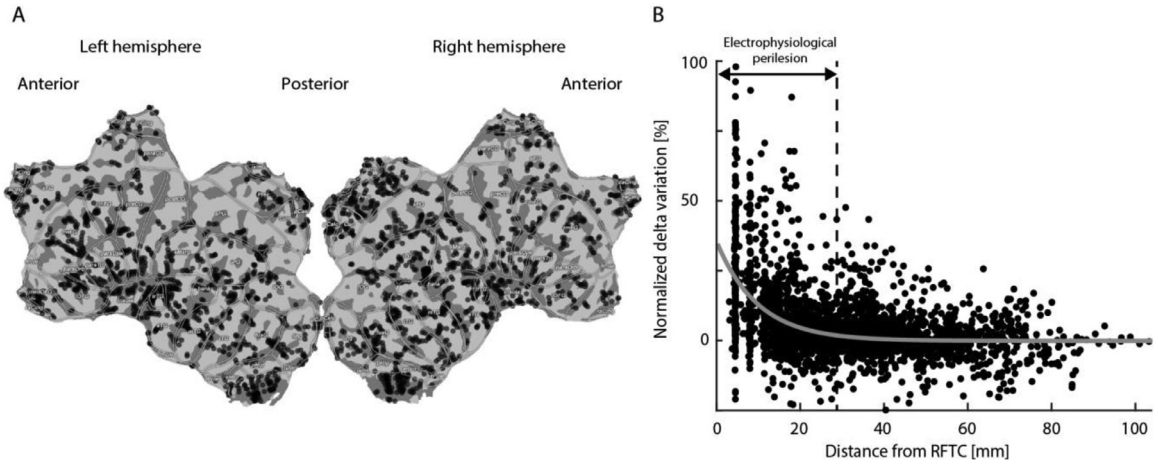

Fig. 2. Group level delta power increase. **Panel A**: Spatial distribution of all SEEG contacts locations (black dots) from all subjects, depicted on a template flatmap (MNI152). **Panel B**: relationship between spectral variations in the delta (0.5–4 Hz) power and distance from the closest RFTC sites (Power-Distance Relationship, PDR) performed at the group level. Each dot corresponds to a contact depicted in Panel a. Dashed vertical line is the upper value of the overlapping area identified by hierarchical clustering (28.74 mm, see results). Grey solid line indicates exponential decay function fit.

2015a). The two selected contiguous contacts are then connected to an RF lesion-generator equipment (NeuroN50 and NeuroN100 with Dixi Medical and Alcis electrodes, respectively) and RFTC is performed by increasing electrical power progressively from 1.5 to 8.32 W within 60 s or 10 s (depending on anatomical caveats – e.g. closeness to vessels) within all the selected epileptogenic sites. For each site, this procedure produces an ellipsoidal lesion with a major radius of 3 mm and a minor radius of 1.5 mm, whose foci correspond to the two contacts in which the current is delivered (Bourdillon et al., 2016). Before and after the thermocoagulation procedure, we recorded on average 12 min (3 to 23) of SEEG spontaneous activity during wakefulness.

2.5. *Pre-processing of spontaneous recordings and sleep scoring*

Data were imported from EEG Nihon Kohden format into Matlab (The MathWorks Inc.) and converted using a customized Matlab-based script. Data underwent linear detrending and high-pass filtering (0.5 Hz, third-order Butterworth filter, zero-phase shift). Bipolar montages were calculated by subtracting the signals from adjacent contacts of the same depth-electrode (166 ± 18 bipolar contacts per subject) to minimise volume conduction and to maximise spatial resolution (Li et al., 2018). Data were visually inspected by trained neurophysiologists, and contacts exhibiting sustained artefactual activity or continuous epileptiform SEEG activity were excluded from further analysis to avoid interference of non-biological and epileptiform discharges on the subsequent quantifications (see Controls for the role of epileptic activity). In addition, contacts selected for delivering RFTC were excluded from further analyses (yellow contacts in Supplementary Fig. 1). The remaining contacts (138 ± 27 per subject – percentage: 82.90 ± 11.18%) used for the physiological investigation underwent further visual inspection in order to mark and remove electrical artefacts and possible, rare paroxysmal waveforms (spikes, spike-wave, sharp-waves, slow epileptic deflections and paroxysmal activity, Supplementary Fig. 2A). The same pre-processing was applied on both wakefulness and sleep recordings. On the latter, off-line sleep scoring was applied using one scalp EEG derivation, together with one bipolar electrooculographic (EOG) and

one electromyographic (EMG) derivation to confirm that all sessions were recorded during NREM N3 (Silber et al., 2007).

2.6. Spectral analysis

For each subject and contact, we quantified the power spectral density (PSD, Fig. 1C) of the SEEG activity recorded before and after RFTC by averaging the PSD of all artefact-free epochs (5 s length, pre-RFTC number of epochs =115 ± 50, post-RFTC number of epochs = 96 ± 56). Each PSD frequency bin was normalised for the average across high frequencies (30–40 Hz) (Nelson et al., 2013) to minimise the effects of local tissue resistance modifications possibly induced by RFTC (Gaetz 2004) – see also Supplementary Fig. 3. To quantify delta power, we averaged PSD bins between 0.5 and 4 Hz. Then we computed the percentage variation of delta power during post- with respect to pre-RFTC (i.e. [post-RFTC – pre-RFTC] / [pre-RFTC] * 100), as shown for example in Fig. 1D. We applied the same procedures to calculate the percentage variation of delta power during NREM sleep with respect to pre-RFTC activity. The relationship between delta power variation and the distance from the RFTC sites was represented by a scatter plot, defined Power-Distance Relationship (PDR), which could be fitted with a negative exponential fit (Fig. 2, Supplementary Fig. 4). Finally, based on the PDR, we operationally defined the extent of the perilesional area (E-perilesion) by applying a hierarchical clustering algorithm (Fig. 2 and Supplementary Fig. 5, Matlab Statistic and machine learning toolbox with automatic number of clusters selection using the Euclidean and Ward distances). This analysis empirically identified two clusters (Supplementary Fig. 5) clearly separated on the x axis (i.e. distance from RFTC) at 28.74 mm. For each subject, single contacts pertaining to each cluster are depicted in Supplementary Fig. 1.

2.7. Pre-processing of cortico-cortical potentials evoked by SPES and effective connectivity evaluation

During the presurgical evaluation and before the RFTC procedure, an extensive effective connectivity evaluation was performed for each and every subject by means of Single Pulse Electrical Stimulation (SPES) and Cortico-Cortical Evoked Potentials (Matsumoto et al., 2017; Trebaul et al., 2018) – see for example Fig. 3. CCEPs were pre-processed using the automatic pipeline described below. The electrical stimulation artefact was removed by applying a Tukey-windowed median filter. Signals were then filtered (0.5 Hz high-pass 3rd order Butterworth filter) and single trials were split based on the inter stimulus interval (−330 ms, +666 ms). Each trial was baseline-corrected, considering baseline from −300 ms to −20 ms before the stimulation, to avoid possible stimulation artefact residuals. SPES delivered with alternate monophasic pulses were separated in positive and negative and analysed independently. Automatic trials rejection to exclude epileptiform abnormalities and electrical artefacts from further analysis was performed as shown in Supplementary Fig. 6, following these steps: (1) for each time sample and single trial, the average of all the trials was subtracted from each trial; (2) to define the pre-stimulus activity, a null distribution was obtained by merging the baseline (−300 ms to −20 ms) of all trials (Usami et al., 2015); (3) trials exceeding the null distribution were identified according to Chebyshev's inequality and (4) if the maximum voltage value across trials exceeded 7σ of the null distribution (corresponding to α=0.05), the corresponding trial was rejected; (5) this process was performed iteratively, excluding at each step the rejected trials (also from the null distribution) until the maximum value didn't exceed the Chebyshev's inequality threshold (Le Van Quyen et al. 2001). After this automatic trial rejection, we quantified the power of the significant ($> 3\sigma$ of the baseline) CCEPs (Matsumoto et al., 2017; Trebaul et al., 2018) elicited by SPES of RFTC contacts. In order to assess the overall strength of the effective connectivity between each recording contact and the RFCT sites we computed the average of the power of CCEPs from all the RFTC sites.

2.8. Slow wave detection and high-frequency modulation

We then assessed the similarities between post-RFTC wakefulness and natural sleep in the 19 subjects with sleep recordings. We first identified those contacts showing a post-RFTC delta power increase comparable to the relative delta power of NREM sleep with respect to pre-RFCT (blue points in Fig. 4B) – i.e. within the inter-quartile range of the NREM sleep delta power distribution (Fig. 4A, right distribution). Next, we applied a standard slow-wave detection algorithm based on zero-crossings and period criteria (Riedner et al., 2007a) on the same contacts. To this end the analysis employed in Riedner et al. was modified to accommodate the fact that the typical negative polarity of the slow waves recorded at the scalp EEG level, could be either positive or negative in the case of intracerebral bipolar montage (Valderrama et al., 2012). Then, we used the median amplitude of the events identified during NREM to set an amplitude threshold for detecting the occurrence of slow waves in both post-RFTC and pre-RFTC wakefulness recordings. To further confirm that the detected events were associated with neuronal events similar to those of sleep-like slow waves, we performed time-frequency analysis to assess the presence of significant suppressions of high frequency activity. As revealed by previous studies in animal and humans, these frequency modulations of the intracranial EEG signal are a reliable extracellular proxy of the periods of neuronal silence (or OFF-periods) characterizing the cortical slow oscillation during sleep (Mukovski et al., 2007; Cash et al., 2009; Csercsa et al., 2010). To demonstrate their co-occurrence with slow waves we first performed a time-frequency analysis at the single contact level in both NREM sleep and post-RFTC conditions (Fig. 4E-F,left), and then we performed a wave-triggered average of the envelope of gamma activity (above 60 Hz), based on the slow wave previously detected (Ray et al., 2008).

2.9. Statistical analysis

Group-level statistical analyses were performed in R using a multilevel approach, due to the clustered nature of the data – i.e. channels within subjects (Aarts et al., 2014). Mixed effects models were employed to test (i) the exponential decay (self-starting non-linear asymptotic regression), (ii) the perilesional normalized delta power increase (linear mixed effects model), (iii) the relationship between normalized delta power, connectivity, and distance (mixed-effects linear regression), and (vi) the number of slow waves across conditions (generalized linear mixed effects). Instead, the modulation of gamma activity within different conditions was tested using a hierarchical bootstrap test as the mixed effects approach failed to converge. A detailed description of the statistical analyses is available in the Supplementary Materials.

2.10. Data availability

All data needed to evaluate the paper's conclusions are present in the paper. Additional data related to this paper may be requested from the corresponding author. Raw data are available on request.

3. Results

3.1. SEEG measurements performed before and after focal brain lesions induced by RFTC

The 21 epileptic patients included in the present work underwent RFTC as preliminary therapeutic treatment. RFTC induces a focal lesion (Fig. 1A) at specific cortical sites identified as epileptogenic or presumably involved in the epileptogenic network (see methods for details). All contacts considered free from epileptic activity (see methods) were used to compare SEEG activity before and after RFTC (Fig. 1B). In addition, several analyses were performed to control for possible influences of epileptic activity in determining the SEEG changes observed after RFTC (see Controls for the role of epileptic activity and Supplementary Fig.

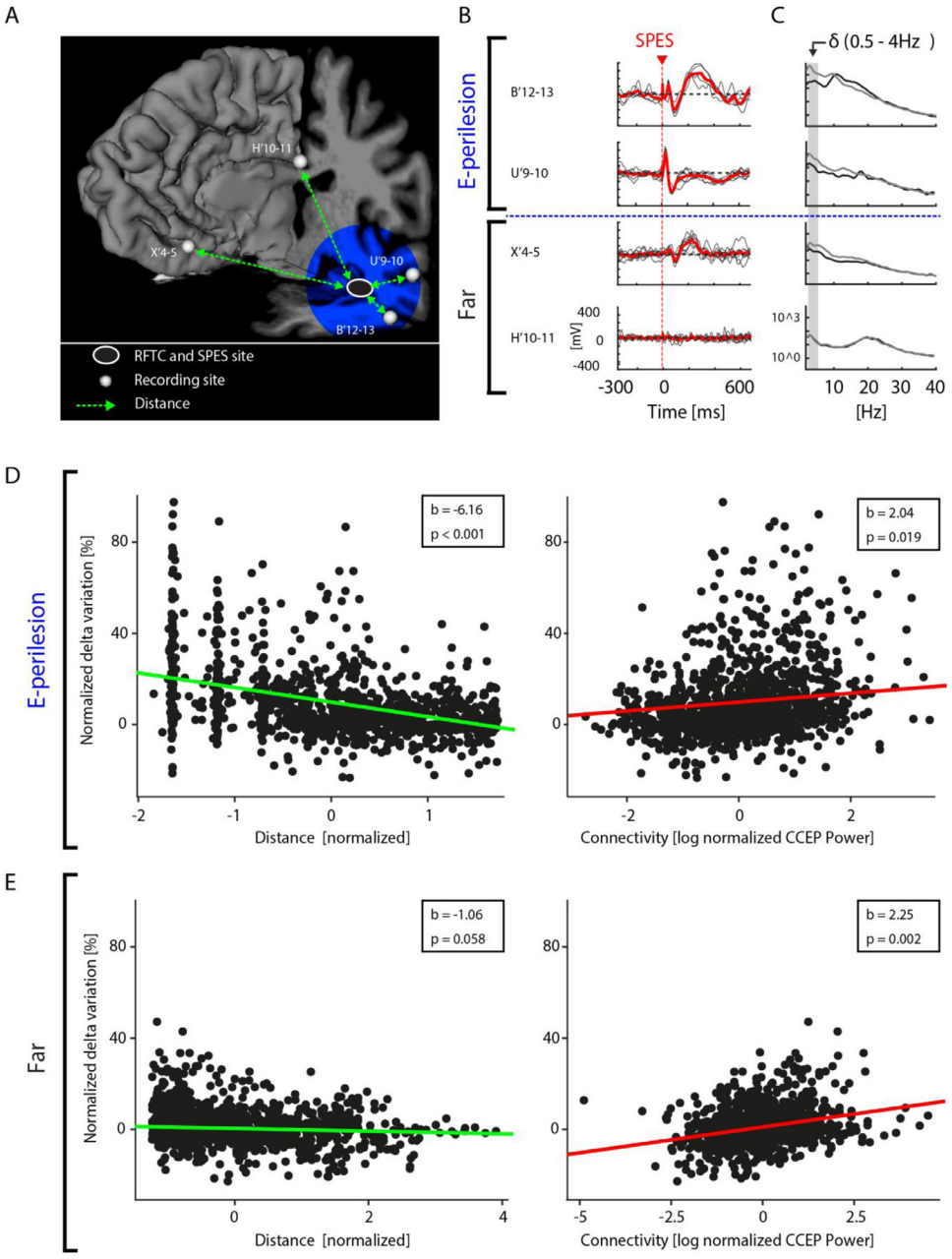

Fig. 3. Relationship between delta increase and connectivity with RFTC areas. **Panel A**: T1 MRI (axial and coronal sections of the left hemisphere) and 3D surface reconstruction (of the right hemisphere) from a representative subject. Dashed green arrows show the distance from one RFTC site (black ovoid, T'6–7, left Superior Temporal gyrus) to four bipolar recording contacts (white points: B'12–13 in the left Middle Temporal gyrus; U'9–10 in the left Superior Temporal gyrus; X'4–5 in the left Medial Orbitofrontal cortex; H'10–11 in the left Rostral Middle Frontal gyrus). The four representative contacts are all located in the left hemisphere and 3D reconstruction of the right hemisphere is show as a reference. Shaded blue area indicates E-perilesion. **Panel B**: For the same contacts depicted in Panel a, the corresponding CCEPs are shown sorted by distance (from top to bottom). **Panel C**: for the same four contacts reported in Panel b, the PSD of pre-RFTC (black) and post-RFTC (grey) activity. **Panel D**: on the left, relationship between delta power (0.5–4 Hz) variations and distance from the nearest RFTC site for each of the recording sites pertaining to E-perilesion. Green line depicts the linear fit using a mixed effect linear regression. On the right, relationship between delta power (0.5–4 Hz) variations average magnitude of CCEPs collected from each of the recording sites within E-perilesion when stimulating RFTC sites. Red line depicts the linear fit using a mixed effect linear regression. **Panel E**: same as Panel d but for contact far from RFTC site (i.e. out of E-perilesion). (For interpretation of the references to colour in this figure legend, the reader is referred to the web version of this article.)

2). After RFTC, the fast frequency activity typical of wakefulness was replaced by slow SEEG activity that was most prominent close to the thermocoagulated area and gradually diminished with distance (Fig. 1B). To quantify these changes, which could be already appreciated by visual inspection, we calculated the PSD (Fig. 1C) of SEEG activity on all artefact-free epochs (see methods for a description of the pre-processing and manual data cleaning procedures) collected both before and after the RFTC procedure (average duration of recordings: 12.97 ± 4.69 min and 12.95 ± 10.65 min, respectively). Computing the percentage variation of delta (0.5–4 Hz) power of post-RFTC with respect to pre-RFTC activity confirmed a gradient decreasing with distance from the RFTC site (Fig. 1D).

3.2. Electrophysiological effects of RFTC extend beyond the area of structural injury

The presence of a spatial gradient of delta power around the lesion was further characterized by a regression analysis (non-linear mixed model) based on all artefact-free contacts from all subjects (Fig. 2A). Specifically, the percentage variation of normalised delta power was represented as a function of distance from the closest RFTC site in a scatter plot that we henceforth call Power-Distance Relationship (PDR). Here, we found that PDR could be fit with an exponential decay function at the group level (Fig. 2B, Supplementary Table 2) and by a negative exponential regression at the single subject level (Supplementary Fig. 4). Although the increase in normalized delta power was not limited to the contacts close to the RFTC and was also visible at distant recording sites (up to 6 cm, see PDR in Fig. 2), we first aimed at defining the extent of the perilesional area characterised by maximal delta increase. This boundary was operationally identified by employing hierarchical cluster analysis. This blind, data-driven procedure allowed demarcating a cluster of contacts within a volume with a radius of 28.74 mm from the RFTC sites, (dashed vertical line in Fig. 2B) henceforth defined as the electrophysiological perilesional area (E-perilesion). In this area, the difference between pre- and post-RFTC delta power was statistically significant as assessed by a linear mixed effects model ($\beta = 0.45$,

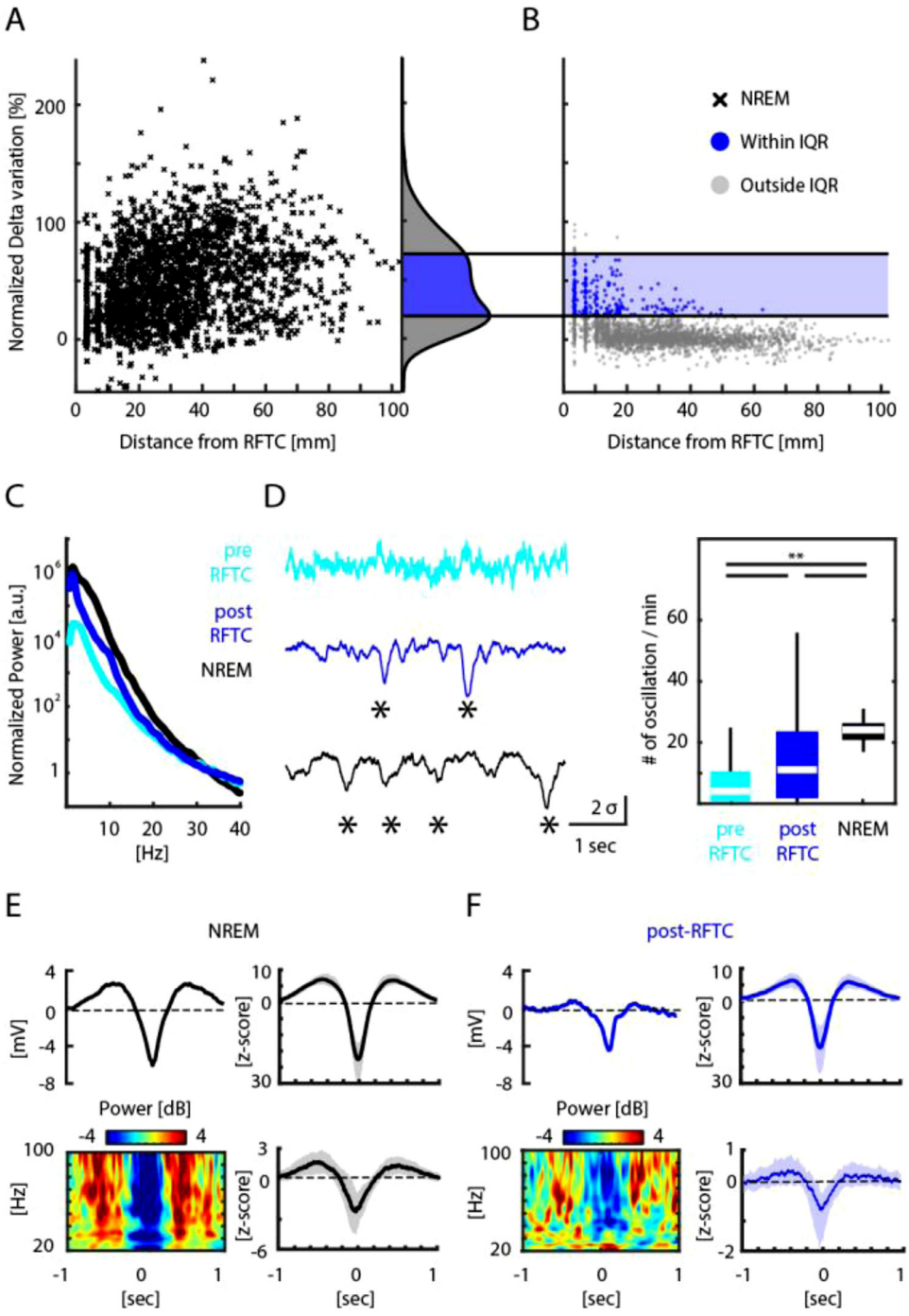

Fig. 4. Sleep-like features of slow waves detected post-RFTC. **Panel A**: On the left, group level PDR obtained by NREM sleep recordings. Black X represents, for each single contact, the relative delta power of NREM sleep with respect to pre-RFTC. On the right, the corresponding probability density with interquartile-range (IQR) highlighted in blue. **Panel B**: Group level PDR. Blue dots indicate contacts showing a delta power increase within the IQR of NREM sleep. Grey dots are all the others. **Panel C**: PSD of SEEG activity from one representative contact during NREM sleep (black), pre-RFTC (cyan trace) and post-RFTC (blue trace). **Panel D**: on the left, representative spontaneous activity (5 s) recorded during NREM sleep (black trace), pre-RFTC (cyan trace) and post-RFTC (blue trace) in wakefulness. Asterisks indicate the detected slow waves. On the right, comparison of the total number of oscillations per minute (in the delta range) detected in the SEEG activity during wakefulness before RFTC (cyan boxplot) and after RFTC (blue) and during NREM sleep (black boxplot) is shown. Asterisks indicate significance values as reported in Table S5. **Panel E**: on the left, average (solid black line, top panel) and time-frequency power spectrum (bottom panel) of the slow waves detected during NREM sleep from one representative contact; on the right, median (solid line, IQR shaded) of all the slow waves (top panel) detected from all subjects during NREM sleep and the corresponding median (solid line, IQR shaded) of the gamma activity modulation (bottom panel). **Panel F**: same as Panel E but for post-RFTC condition. (For interpretation of the references to colour in this figure legend, the reader is referred to the web version of this article.)

$p < 0.001$, $R^2_c = 0.32$; see Supplementary Table 3 for a complete report of the model's estimates and statistical results). Notably, the E-perilesion (radius 28.74 mm) identified by data-driven clustering exceeded by almost 10 times the size of the typical structural lesion (an ovoid with radius ~ 3 mm) described by previous studies employing RFTC with the same parameters used in the present work (Cossu et al., 2015a; Bourdillon et al., 2016, 2017).

3.3. Whole-brain delta power increase correlates with effective connectivity from RFTC sites

While the cluster analysis allowed operationalizing E-perilesion as a volume of strong electrophysiological alterations extending around the RFTC structural lesion, the changes in delta power could often deviate from the fit of the power-distance relationship. Indeed, as evident in Fig. 2B, a number of remote contacts (located up to 6 cm away from the centroid of the lesion) showed a marked increase in delta power. We thus tested the hypothesis that this increase may reflect preferential connections from the RFTC region, above and beyond distance *per se* (Fig. 3A). To this end, we retrospectively pre-processed and analysed the pre-RFTC Cortico-Cortical Evoked Potentials (CCEPs) obtained from 20 subject (CCEPs of subject n.11 not available) by means of Single-Pulse Electrical Stimulation (SPES; Fig. 3B) performed at each RFTC site (Supplementary Fig. 6). Briefly, the power of the evoked response at each recording site was averaged across RFTC sites to obtain the mean connectivity value with respect to the ensemble of all thermocoagulated areas for each recording contact (see methods for details). The relationship between distance from RFTC site, connectivity, and delta power increase is exem-

plified in Fig. 3. Through this analysis, we found that, while within the E-perilesion most contacts featured prominent increases in delta power that correlated with both distance and CCEPs magnitude, this was not the case for contacts far from the RFTC site; out of the E-perilesion, the increase in delta power depended on the magnitude of CCEPs, rather than on geometric distance *per se*. These observations were quantified at the group level by employing, for each cluster (i.e. E-perilesion and far), a mixed effects linear regression analysis using delta power increase as dependant variables and distance and connectivity as predictors (see methods). This analysis showed that, while both connectivity and distance were significant predictors of delta power increase within the E-perilesion (β connectivity = 2.04, $p < 0.05$; β distance = −6.16, $p < 0.001$; R^2_m= 0.20, R^2_c= 0.38; Fig. 3D, Table S4, Supplementary Fig. 7), only connectivity maintained its predictive power far from the RFTC site (β connectivity = 2.25, $p < 0.01$; β distance = −1.06, $p = 0.06$; R^2_m= 0.11, R^2_c= 0.52; Fig. 3E, Table S5, Supplementary Fig. 8). This is consistent with the general notion that the connectome is characterised by preferential patterns of long–range connectivity and with the view of diaschisis as a network-specific phenomenon (Fornito et al., 2015).

3.4. Delta power increase is associated with sleep-like slow waves and OFF-periods

We finally asked whether the observed significant increase in delta power reflected the occurrence of local sleep-like dynamics during wakefulness. To test this hypothesis, we compared the SEEG activity recorded both pre- and post-RFTC with that collected during periods of sleep recorded in the same subjects and contacts. The comparison between post-RFTC and NREM sleep delta power revealed the presence of contacts ($n = 250$, ~10%) in which post-RFTC wakefulness delta power increased to levels comparable to those of NREM sleep – i.e. within the Inter-Quartile Range (IQR) of the delta power increase of NREM sleep (Fig. 4A-C – see methods for details). We then asked whether, for these contacts, post-RFTC delta power increase reflected the occurrence of slow waves (Fig. 4D), according to criteria defined by previous sleep studies (Mukovski et al., 2007; Cash et al., 2009). First, we applied a period-amplitude detection algorithm (see Methods) to identify sleep slow waves in NREM sleep recordings. Then, we used the median amplitude of these events to set a threshold for the identification of sleep-like slow-waves in both post- and pre-RFTC wakefulness recordings. As shown in Fig. 4D, we found that the slow-wave density (oscillations per minute) in post-RFTC condition (13.5 ± 13.5) was significantly higher than pre-RFTC condition (7.58±8.46; $p < 0.001$) albeit lower than NREM sleep (23.2 ± 2.89; $p < 0.01$), as confirmed by a zero-inflated Poisson generalized linear mixed effects model (R^2_m=0.32, R^2_c=0.72; see Supplementary Table 6).

Finally, we assessed whether the post-RFTC significant increase in both delta power and number of slow waves was associated with the occurrence of neuronal OFF-periods, the hallmark of sleep slow waves.

A wave-triggered average analysis on the slow waves detected in the post-RFTC perilesional contacts revealed a significant ($p<0.001$, hierarchical bootstrap test, Supplementary Table 7) modulation of high-frequency (> 60 Hz) activity (Steriade et al., 1993; Amzica and Steriade 1998; Mukovski et al., 2007; Cash et al., 2009) similar to one observed during NREM sleep ($p<0.001$, hierarchical bootstrap test, Table S8), suggesting the occurrence of neuronal OFF-periods, associated with post-RFTC slow waves (Fig. 4F, see Methods for details) (Mukovski et al., 2007; Cash et al., 2009).

3.5. Controls for the role of epileptic activity

We applied manual rejection of all epochs and contacts containing pathological activity – such as spikes, spike-and-waves, paroxysmal discharges, and epileptic slow deflections. (see Supplementary Fig. 2A) - in order minimize the impact of SEEG abnormalities on our observations. In addition to this standard procedure, we performed a set of specific controls to verify that the occurrence of slow waves and their propagation after RFTC did not depend on ongoing pathological activity nor on pre-existing network alterations. First, we verified that the increase in delta power did not correlate with the frequency of epileptic activity detected after RFTC at the level of each recording site (Supplementary Fig. 2B), thus excluding a role SEEG abnormalities in determining the observed spectral changes. Second, we performed the same analysis with respect to the spatial distribution of epileptic activity detected before RFTC to control for the possible influence of pre-existing network alterations (Supplementary Fig. 2C). Third, we verified that the delta increase did not depend on whether RFTC was performed on a contact pertaining to the epileptogenic zone (EZ, as defined by spontaneous ictal recordings and/or clinical outcomes) or on a contact pertaining to an early-propagation zone (EPZ; defined as the area of early propagation of ictal discharges, Supplementary Fig. 2D) (Bartolomei et al., 2017). Fourth, we verified that our results were not related to the presence of specific underlying aetiology - such as periventricular nodular heterotopia (Battaglia et al., 2006) and temporal lobe epilepsy with or without Hippocampus sclerosis (Weng et al., 2020) - that are known to be associated with altered thalamocortical connectivity (see MRI and diagnosis in Supplementary Table 1). In line with this, since epileptic disorders associated to structural lesions are known to induce network modifications, we also verified that all our results could be confirmed when including only MRI negative subjects (i.e. no structural lesions) in the statistical analyses.

Fifth, we verified that contacts showing sleep-like activity after RFTC did not show a priori high narrow-band 3–4 Hz power possibly indicating pathological activity (Supplementary Fig. 2E-F, linear mixed regression and linear mixed model analysis). Sixth, along the same line we compared the pre-RFTC spectral profile between contacts showing sleep-like delta increase after RFTC and contacts that did not showed an increase and we found no differences (Supplementary Fig. 2G, Wilcoxon rank sum test, FDR corrected). Finally, we verified that the sleep-like events detected after RFTC showed a similar morphology to physiological sleep slow waves and that both showed a different morphology with respect to epileptic slow deflections (Nir, 2011). Indeed, based on the knowledge that sleep-slow-waves tend to be more symmetric while epileptic events are typically asymmetric (Riedner et al., 2007b; Nir et al., 2011) we compared the slopes of the detected events across conditions (Supplementary Fig. 2H-J). With this analysis, we found that Post-RFTC events and sleep events were not different between them ($p = 0.83$; $p = 0.72$), but both differed from the epileptic benchmark ($p<0.01$).

4. Discussion

By providing a high-resolution intracerebral assessment of the local and network-level consequences of controlled cortical lesions, the present work provides direct evidence for electrophysiological diaschisis in humans. As revealed by the comparison between pre- and post-RFTC cortical activity, brain lesions induced an increase in the amplitude and number of slow waves, which was unrelated to epileptic alterations. Crucially, these slow waves intruding within wakefulness were comparable to those occurring during NREM sleep, were prominent within the perilesional area, and could percolate to distant sites through specific connectivity patterns, above and beyond the anatomical distance *per se*.

4.1. Generation of perilesional sleep-like slow waves

Microinvasive surgery, such as RFTC, results in focal brain lesions that are not associated with significant vascular alterations and whose localisation and extent can be precisely controlled (Cossu et al., 2015a). So far, the effects of RFTC have been quantified by means of morphological observations (Bourdillon et al., 2016; Garbelli et al., 2016). Typically (Bourdillon et al., 2016), the extension of the structural damage induced by a RFTC through a pair of contacts is on average an ovoid with radii

of 1.5 mm and 3 mm. The first important finding of the present study is a significant increase of delta power in an area surrounding the RFTC site. This effect, which steeply decayed from the centroid of the lesion (Fig. 1, Fig. 2 and Supplementary Fig. 1), identified a perilesional area extending to a radius of 28 mm – an order of magnitude larger than that of the structural lesion.

Various factors may explain this perilesional effect. First, local oedema, as observed in animal models (Clasen et al., 1958; Schaul et al., 1976) can lead to a failure of sodium-potassium pumps and ionic unbalances that facilitate the expression of delta activity (Rabiller et al., 2015). This mechanism plays a relevant role in the acute phases of brain damage, but in the case of RFTC it should be limited to a thin layer (<1 mm) of brain tissue surrounding the RFTC area, as suggested by inflammation- and oedema-related histological signs (Garbelli et al., 2016). A second factor that can enable the expression of slow waves in the E-perilesion is the lack of input from ascending activating systems due to damage of white matter fibres (McCormick et al., 1991). This mechanism has been thoroughly documented by animal experiments (Nita et al., 2007) in which the lesion involves to the underlying white matter, such as in the case of RFTC. A third, important mechanism leading to the expression of neuronal OFF-periods and slow oscillations is an unbalance between excitation and inhibition (Funk et al., 2017), due to the disruption of lateral cortico-cortical excitatory connections (Weliky et al., 1995; Timofeev 2000; Boucsein et al., 2011). In all cases, the present high-resolution intracranial exploration, demonstrating the appearance of sleep-like slow waves in a large area surrounding the lesion, explains the early macroscale observation of EEG slowing (Nuwer et al., 1987a; Butz et al., 2004; Poryazova et al., 2015; Cassidy et al., 2020) as well as recent TMS-EEG evidence of altered reactivity (Sarasso et al., 2020; Tscherpel et al., 2020) in the lesioned hemisphere of stroke patients.

4.2. Percolation of slow waves through large-scale networks

The reappearance of slow waves at distant sites well beyond the perilesional area cannot be explained by local phenomena such as oedema or direct disruption of local connections by the lesion. The present results suggest that these instances can be predicted by specific patterns of long-range effective connectivity as assessed in individual subjects from a causal perspective by means of CCEPs (Matsumoto et al., 2017; Trebaul et al., 2018). Indeed, while close to the lesion both geometrical distance and connectivity were significant predictors of delta increase, with a relative higher weight for distance, outside of E-perilesion effective connectivity clearly outperformed geometrical distance (Fig. 3). This result provides the first direct electrophysiological evidence of a selective network-level alteration of neural activity after cortical lesion, in line with the classic definition of diaschisis. Hence, the intrusion and long-range percolation of sleep-like slow waves at specific nodes of the network reported here provides direct empirical support to the original hypothesis of a remote functional disruption in regions connected to site of focal lesion (Feeney and Baron 1986) through cortico-cortical and/or cortico-subcortical connections (McCormick and Bal 1997; Crunelli and Hughes 2010).

Whether distant slow waves occur because of the propagation of activity from the perilesional area or because of lack of excitatory input from the lesioned site remains an interesting open question. In principle both mechanisms are plausible. Indeed, physiological sleep slow waves have been shown to propagate from a generator to distant sites through existing anatomical connections (Volgushev et al., 2006), potentially following previously existing anatomical and functional pathways (Zhang et al., 2018; Silverstein et al., 2020). On the other hand, deafferentation can lead to both enhanced slow waves and a reduction of high frequency activity (Timofeev 2000). While the delta power increase occurred also in the absolute spectrum (Supplementary Figure 3), it would be interesting for future studies to systematically explore the presence of a concomitant reduction of high frequencies, which was precluded here by the present normalization strategy.

4.3. Implications of local sleep after focal brain injury

Intracerebral studies performed in sleep-deprived rodents and humans have shown that slow waves and neuronal OFF-periods can occur locally and at specific cortical sites in the context of an awake brain (Nobili et al., 2012) leading to selective motor impairment or cognitive lapses depending on the region of the cortex involved (Vyazovskiy et al., 2011; Nir et al., 2017). Subjects undergoing RFTC can benefit from the procedure and rarely show neuropsychological or neurological deficits, possibly due to the fact that the lesions are small and deliberately performed in areas that are identified as functionally non-primary (Cossu et al., 2015a; Bourdillon et al., 2017). Within the constraints imposed by the clinical procedure, it will be important for future studies to assess subjects behaviourally in both baseline conditions and post-RFTC with a fine-grained battery of motor/cognitive tests, tailored on the specific brain areas and networks involved by the RFTC. The present demonstration that even small lesions can lead to the intrusion of local sleep-like slow waves and OFF-periods at the network level bears important implications. For example, it is known that the consequences of microinfarctions in humans may range from cognitive sparing to dementia but the reason for this large discrepancy is unclear; an interesting possibility is that the induction of pathological slow waves in intact portions of the cortex following microinfarctions may have unpredictable, magnifying effects at the network level in the brain of some subjects with multiple microvascular lesions. All the more so, the electrophysiological mechanism described here is expected to play a major role in subjects suffering from larger lesions, such as stroke subjects. In these patients, TMS-EEG studies have revealed sleep-like stereotypical responses associated with impairment of information processing in the perilesional area (Sarasso et al., 2020; Tscherpel et al., 2020) and EEG recordings often detect slowing extending to the contralateral hemisphere (Nuwer et al., 1987b). Linking the intrusion of sleep-like events in the awake brain to focal injury is very important, given the complex nature of the effects that slow waves can have on cortical circuits. For example, the occurrence of slow waves and the associated silent OFF-periods are known to affect information processing, impairing cognitive and motor functions (Vyazovskiy et al., 2011; Nir et al., 2017). Further, they can interfere with the propagation of higher-frequency travelling waves, potentially impairing the related cognitive abilities (Zhang et al., 2018). On the other hand, slow waves and OFF periods can also exert beneficial, protective effects (Pace et al., 2015; Cassidy et al., 2020) and are known to play a role in shaping and remodelling cortical connections (Buzsáki 1998; Tononi and Cirelli 2014). To add a layer of complexity, this remodelling effects can positively or negatively impact the cognitive functions depending on what kind of slow waves are occurring; for example, Kim and colleagues have recently shown that single slow waves and sustained delta activity have competing roles in memory consolidation processes (Kim et al., 2019).

In this context, the present findings trigger a number of interesting questions. What is the true nature of slow wave activity following brain injury? Are slow waves just a detrimental side effect altering network activity above and beyond the structural damage? Are they instead the price to pay for energy saving and/or circuits remodelling after brain injury? One interesting possibility is that slow waves might be protective and beneficial in the acute recovery phase and then become detrimental if they persist indefinitely into the chronic phase . Importantly, acute and chronic slow waves may be originated by different pathogenetic mechanisms; while inflammatory cytokines are likely to play a role in the acute phase (Krueger and Majde 1995), chronic slow waves are more likely to be caused, amongst other factors, by an alteration of the excitation/inhibition balance (Takeuchi and Izumi 2012). The present mesoscale exploration may help addressing these questions by bridging microscale animal experiments to macroscale EEG and neu-

roimaging findings in human subjects. Ultimately, linking the engagement of cortical sleep-like dynamics to focal brain injury provides an electrophysiological mechanism for diaschisis and may open new therapeutic venues, including the possibility of conditioning the evolution of stroke rehabilitation by dampening or enhancing slow waves in specific time windows.

Acknowledgments

We are grateful to Chiara Cirelli, Mario Rosanova, Matteo Fecchio, and Michele Colombo for their comments and suggestions.

Funding

This research has received funding from the European Union's Horizon 2020 Framework Programme for Research and Innovation under the Specific Grant Agreement No. 720270 (Human Brain Project SGA1- to M.M. and S.F.), No. 785907 (Human Brain Project SGA2 - to M.M. and S.F.), and No. 945539 (Human Brain Project SGA3 - to M.M.). The study has also been partially funded by the grant "Sinergia" CRSII3_160803/1 of the Swiss National Science Foundation (to M.M. and C.L.A.B.) and by the James S. McDonnell Foundation Scholar Award 2013 and the Tiny Blue Dot Foundation (to M.M.).

Credit author statement

Authors Contribution: Conceptualization: S.R., A.P., S.S., I.S. and M.M.; supervision: G.lR, C.B., M.M.; data curation: S.R., A.P., A.R., F.Z., S.P. and I.S.; investigation: L.N., S.F., L.T., P.dO., G.lR. and I.S.; formal analysis: S.R., E.M., and A.C.; writing original draft: A.P., S.R, E.M., S.P., S.S., and M.M; review and editing: all authors.

Data and code availability statement

All data needed to evaluate the paper's conclusions are present in the paper. Additional data related to this paper may be requested from the corresponding author. Raw data are available on request, upon proper anonymization. Code is available on request.

Supplementary materials

Supplementary material associated with this article can be found, in the online version, at doi:10.1016/j.neuroimage.2021.117964.

References

Aarts, E., Verhage, M., Veenvliet, J.V., Dolan, C.V., van der Sluis, S., 2014. A solution to dependency: using multilevel analysis to accommodate nested data. Nat. Neurosci. 17, 491–496.

Amzica, F., Steriade, M., 1998. Electrophysiological correlates of sleep delta waves. Electroencephalogr. Clin. Neurophysiol. 107, 69–83.

Avants, B.B., Tustison, N.J., Song, G., Cook, P.A., Klein, A., Gee, J.C., 2011. A reproducible evaluation of ANTs similarity metric performance in brain image registration. Neuroimage 54, 2033–2044.

Baldassarre, A., Ramsey, L.E., Siegel, J.S., Shulman, G.L., Corbetta, M., 2016. Brain connectivity and neurological disorders after stroke. Curr. Opin. Neurol. 29, 706–713.

Bartolomei, F., Lagarde, S., Wendling, F., McGonigal, A., Jirsa, V., Guye, M., Bénar, C., 2017. Defining epileptogenic networks: contribution of SEEG and signal analysis. Epilepsia 58, 1131–1147.

Battaglia, G., Chiapparini, L., Franceschetti, S., Freri, E., Tassi, L., Bassanini, S., Villani, F., Spreafico, R., D'Incerti, L., Granata, T, 2006. Periventricular nodular heterotopia: classification, epileptic history, and genesis of epileptic discharges. Epilepsia 47, 86–97.

Boucsein, C., Nawrot, M., Schnepel, P., Aertsen, A., 2011. Beyond the cortical column: abundance and physiology of horizontal connections imply a strong role for inputs from the surround. Front. Neurosci. 5.

Bourdillon, P., Isnard, J., Catenoix, H., Montavont, A., Rheims, S., Ryvlin, P., Ostrowsky–Coste, K., Mauguiere, F., Guénot, M., 2016. Stereo-electro-encephalography–guided radiofrequency thermocoagulation: from in vitro and in vivo data to technical guidelines. World Neurosurg.

Bourdillon, P., Isnard, J., Catenoix, H., Montavont, A., Rheims, S., Ryvlin, P., Ostrowsky-Coste, K., Mauguiere, F., Guénot, M., 2017. Stereo electroencephalography-guided radiofrequency thermocoagulation (SEEG-guided RF-TC) in drug-resistant focal epilepsy: results from a 10-year experience. Epilepsia 58, 85–93.

Buchkremer-Ratzmann, I., August, M., Hagemann, G., Witte, O.W., 1996. Electrophysiological transcortical diaschisis after cortical photothrombosis in rat brain. Stroke 27, 1105–1111.

Butz, M., Gross, J., Timmermann, L., Moll, M., Freund, H.-J., Witte, O.W., Schnitzler, A., 2004. Perilesional pathological oscillatory activity in the magnetoencephalogram of patients with cortical brain lesions. Neurosci. Lett. 355, 93–96.

Buzsáki, G., 1998. Memory consolidation during sleep: a neurophysiological perspective. J. Sleep Res. 7 (Suppl 1), 17–23.

Cardinale, F., Rizzi, M., Vignati, E., Cossu, M., Castana, L., d'Orio, P., Revay, M., Costanza, M.D., Tassi, L., Mai, R., Sartori, I., Nobili, L., Gozzo, F., Pelliccia, V., Mariani, V., Lo Russo, G., Francione, S, 2019. Stereoelectroencephalography: retrospective analysis of 742 procedures in a single centre. Brain J Neurol 142, 2688–2704.

Carmichael, S.T., Tatsukawa, K., Katsman, D., Tsuyuguchi, N., Kornblum, H.I., 2004. Evolution of diaschisis in a focal stroke model. Stroke 35, 758–763.

Carrera, E., Tononi, G., 2014. Diaschisis: Past, Present, Future. Oxford University Press.

Carter A.R., Shulman G.L., Corbetta M. 2012. Why use a connectivity-based approach to study stroke and recovery of function? Neuroimage. 2012 Oct 1;62(4):2271-80. doi:10.1016/j.neuroimage.2012.02.070. Epub 2012 Mar 5.

Cash, S.S., Halgren, E., Dehghani, N., Rossetti, A.O., Thesen, T., Wang, C., Devinsky, O., Kuzniecky, R., Doyle, W., Madsen, J.R., Bromfield, E., Eross, L., Halász, P., Karmos, G., Csercsa, R., Wittner, L., Ulbert, I., 2009. The human K-complex represents an isolated cortical down-state. Science 324, 1084–1087.

Cassidy, J.M., Wodeyar, A., Wu, J., Kaur, K., Masuda, A.K., Srinivasan, R., Cramer, S.C., 2020. Low-frequency oscillations are a biomarker of injury and recovery after stroke. Stroke 51, 1442–1450.

Clasen, R.A., Cooke, P.M., Martin, F.A., Williams, J.R., Hass, G.M., 1958. Cerebral edema and electroencephalographic changes after local acute closed cerebral injury. AMA Arch. Neurol. Psychiatry 80, 696–707.

Cossu, M., Fuschillo, D., Casaceli, G., Pelliccia, V., Castana, L., Mai, R., Francione, S., Sartori, I., Gozzo, F., Nobili, L., Tassi, L., Cardinale, F., Lo Russo, G, 2015a. Stereoelectroencephalography-guided radiofrequency thermocoagulation in the epileptogenic zone: a retrospective study on 89 cases. J. Neurosurg. 123, 1358–1367.

Cossu, M., Fuschillo, D., Casaceli, G., Pelliccia, V., Castana, L., Mai, R., Francione, S., Sartori, I., Gozzo, F., Nobili, L., Tassi, L., Cardinale, F., Lo Russo, G, 2015b. Stereoelectroencephalography-guided radiofrequency thermocoagulation in the epileptogenic zone: a retrospective study on 89 cases. J. Neurosurg. 123, 1358–1367.

Crunelli, V., Hughes, S.W., 2010. The slow (<1Hz) rhythm of non-REM sleep: a dialogue between three cardinal oscillators. Nat. Neurosci. 13, 9–17.

Csercsa, R., Dombovári, B., Fabó, D., Wittner, L., Erss, L., Entz, L., Sólyom, A., Rásonyi, G., Szcs, A., Kelemen, A., Jakus, R., Juhos, V., Grand, L., Magony, A., Halász, P., Freund, T.F., Maglóczky, Z., Cash, S.S., Papp, L., Karmos, G., Halgren, E., Ulbert, I., 2010. Laminar analysis of slow wave activity in humans. Brain 133, 2814–2829.

Dimova, P., de Palma, L., Job-Chapron, A.-.S., Minotti, L., Hoffmann, D., Kahane, P, 2017. Radiofrequency thermocoagulation of the seizure-onset zone during stereoelectroencephalography. Epilepsia 58, 381–392.

Falcon, M.I., Riley, J.D., Jirsa, V., McIntosh, A.R., Chen, E.E., Solodkin, A, 2016. Functional mechanisms of recovery after chronic stroke: modeling with the virtual brain. eNeuro 3, 202–208.

Feeney, D.M., Baron, J.C., 1986. Diaschisis. Stroke. 17, 817–830.

Fischl B. 2012. FreeSurfer. NeuroImage. 2012 Aug 15;62(2):774-81. doi:10.1016/j.neuroimage.2012.01.021. Epub 2012 Jan 10.

Fornito, A., Zalesky, A., Breakspear, M., 2015. The connectomics of brain disorders. Nat. Rev. Neurosci. 16, 159–172.

Funk, C.M., Peelman, K., Bellesi, M., Marshall, W., Cirelli, C., Tononi, G., 2017. Role of somatostatin-positive cortical interneurons in the generation of sleep slow waves. J. Neurosci. Off J. Soc. Neurosci. 37, 9132–9148.

Gaetz, M., 2004. The neurophysiology of brain injury. Clin. Neurophysiol. Off. J. Int. Fed Clin. Neurophysiol. 115, 4–18.

Gao, J.S., Huth, A.G., Lescroart, M.D., Gallant, J.L., 2015. Pycortex: an interactive surface visualizer for fMRI. Front. Neuroinformat. 9.

Garbelli, R., Spreafico, R., Barbaglia, A., Rossini, L., Milesi, G., Zucca, I., Cossu, M., Bramerio, M., Tassi, L., 2016. Stereo-EEG, radiofrequency thermocoagulation and neuropathological correlations in a patient with MRI-negative type IIb focal cortical dysplasia. Seizure 41, 1–3.

Gloor, P., Ball, G., Schaul, N., 1977. Brain lesions that produce delta waves in the EEG. Neurology 27, 326–333.

Guénot, M., Isnard, J., Ryvlin, P., Fischer, C., Mauguière, F., Sindou, M., 2004. SEEG-guided RF thermocoagulation of epileptic foci: feasibility, safety, and preliminary results. Epilepsia 45, 1368–1374.

Keller, C.J., Bickel, S., Entz, L., Ulbert, I., Milham, M.P., Kelly, C., Mehta, A.D., 2011. Intrinsic functional architecture predicts electrically evoked responses in the human brain. Proc. Natl. Acad. Sci. 108, 10308–10313.

Kim, J., Gulati, T., Ganguly, K., 2019. Competing roles of slow oscillations and delta waves in memory consolidation versus forgetting. Cell 179, 514–526 e13.

Krueger, J.M., Majde, J.A., 1995. Cytokines and sleep. Int. Arch. Allergy Immunol. 106, 97–100.

Le Van Quyen, M., Martinerie, J., Navarro, V., Boon, P., D'Havé, M., Adam, C., Renault, B., Varela, F., Baulac, M, 2001. Anticipation of epileptic seizures from standard EEG recordings. Lancet Lond. Engl. 357, 183–188.

Leemburg, S., Gao, B., Cam, E., Sarnthein, J., Bassetti, C.L, 2018. Power spectrum slope is related to motor function after focal cerebral ischemia in the rat. Sleep 41.

Levasseur, M., Baron, J.C., Sette, G., Legault-Demare, F., Pappata, S., Mauguière, F., Benoit, N., Tran Dinh, S., Degos, J.D., Laplane, D, 1992. Brain energy metabolism in bilateral paramedian thalamic infarcts. A positron emission tomography study. Brain J. Neurol. 115 (Pt 3), 795–807.

Li, G., Jiang, S., Paraskevopoulou, S.E., Wang, M., Xu, Y., Wu, Z., Chen, L., Zhang, D., Schalk, G., 2018. Optimal referencing for stereo-electroencephalographic (SEEG) recordings. Neuroimage 183, 327–335.
Matsumoto, R., Kunieda, T., Nair, D., 2017. Single pulse electrical stimulation to probe functional and pathological connectivity in epilepsy. Seizure 44, 27–36.
McCormick, D.A., Bal, T., 1997. Sleep and arousal: thalamocortical mechanisms. Annu. Rev. Neurosci. 20, 185–215.
McCormick, D.A., Pape, H.C., Williamson, A., 1991. Actions of norepinephrine in the cerebral cortex and thalamus: implications for function of the central noradrenergic system. Prog. Brain Res. 88, 293–305.
Mukovski, M., Chauvette, S., Timofeev, I., Volgushev, M., 2007. Detection of active and silent states in neocortical neurons from the field potential signal during slow-wave sleep. Cereb Cortex 17, 400–414.
Narizzano, M., Arnulfo, G., Ricci, S., Toselli, B., Tisdall, M., Canessa, A., Fato, M.M., Cardinale, F, 2017. SEEG assistant: a 3DSlicer extension to support epilepsy surgery. BMC Bioinformat. 18.
Nelson, A., Faraguna, U., Zoltan, J., Tononi, G., Cirelli, C., Nelson, A.B., Faraguna, U., Zoltan, J.T., Tononi, G., Cirelli, C., 2013. Sleep patterns and homeostatic mechanisms in adolescent mice. Brain Sci. 3, 318–343.
Nir, Y., Andrillon, T., Marmelshtein, A., Suthana, N., Cirelli, C., Tononi, G., Fried, I., 2017. Selective neuronal lapses precede human cognitive lapses following sleep deprivation. Nat. Med. 23, 1474–1480.
Nir, Y., Staba, R.J., Andrillon, T., Vyazovskiy, V.V., Cirelli, C., Fried, I., Tononi, G., 2011. Regional slow waves and spindles in human sleep. Neuron 70, 153–169.
Nita, D.A., Cissé, Y., Timofeev, I., Steriade, M., 2007. Waking–sleep modulation of paroxysmal activities induced by partial cortical deafferentation. Cereb Cortex 17, 272–283.
Nobili, L., De Gennaro, L., Proserpio, P., Moroni, F., Sarasso, S., Pigorini, A., De Carli, F., Ferrara, M., 2012. Local aspects of sleep: observations from intracerebral recordings in humans. Progress in Brain Research.
Nuwer, M.R., Jordan, S.E., Ahn, S.S., 1987a. Evaluation of stroke using EEG frequency analysis and topographic mapping. Neurology 37, 1153–1159.
Nuwer, M.R., Jordan, S.E., Ahn, S.S., 1987b. Evaluation of stroke using EEG frequency analysis and topographic mapping. Neurology 37, 1153–1159.
Pace, M., Baracchi, F., Gao, B., Bassetti, C., 2015. Identification of sleep-modulated pathways involved in neuroprotection from stroke. Sleep 38, 1707–1718.
Poryazova, R., Huber, R., Khatami, R., Werth, E., Brugger, P., Barath, K., Baumann, C.R., Bassetti, C.L., 2015. Topographic sleep EEG changes in the acute and chronic stage of hemispheric stroke. J. Sleep Res. 24, 54–65.
Price, C.J., Warburton, E.A., Moore, C.J., Frackowiak, R.S.J., Friston, K.J., 2001. Dynamic diaschisis: anatomically remote and context-sensitive human brain lesions. J. Cogn. Neurosci. 13, 419–429.
Rabiller, G., He, J.W., Nishijima, Y., Wong, A., Liu, J., 2015. Perturbation of Brain Oscillations after Ischemic stroke: A Potential Biomarker for Post-Stroke Function and Therapy. MDPI AG.
Ray, S., Crone, N.E., Niebur, E., Franaszczuk, P.J., Hsiao, S.S., 2008. Neural correlates of high-gamma oscillations (60-200 Hz) in macaque local field potentials and their potential implications in electrocorticography. J. Neurosci. 28, 11526–11536.
Riedner, B.A., Vyazovskiy, V.V., Huber, R., Massimini, M., Esser, S., Murphy, M., Tononi, G., 2007a. Sleep homeostasis and cortical synchronization: III. A high-density EEG study of sleep slow waves in humans. Sleep 30, 1643–1657.
Riedner, B.A., Vyazovskiy, V.V., Huber, R., Massimini, M., Esser, S., Murphy, M., Tononi, G., 2007b. Sleep homeostasis and cortical synchronization: III. A high-density EEG study of sleep slow waves in humans. Sleep 30, 1643–1657.
Rorden, C., Karnath, H.O., 2004. Using human brain lesions to infer function: a relic from a past era in the fMRI age? Nat. Rev. Neurosci. 5, 812–819.
Saenger, V.M., Ponce-Alvarez, A., Adhikari, M., Hagmann, P., Deco, G., Corbetta, M., 2018. Linking entropy at rest with the underlying structural connectivity in the healthy and Lesioned brain. Cereb Cortex 28, 2948–2958 N Y N 1991.
Sarasso, S., D'Ambrosio, S., Fecchio, M., Casarotto, S., Viganò, A., Landi, C., Mattavelli, G., Gosseries, O., Quarenghi, M., Laureys, S., Devalle, G., Rosanova, M., Massimini, M, 2020. Local sleep-like cortical reactivity in the awake brain after focal injury. Brain J. Neurol. 143, 3672–3684.
Schaul, N., Ball, G., Gloor, P., Pappius, H.M., 1976. The EEG in Cerebral Edema. In: Dynamics of Brain Edema. Springer, pp. 144–149.
Scholly, J., Pizzo, F., Timofeev, A., Valenti-Hirsch, M.P., Ollivier, I., Proust, F., Roehri, N., Bénar, C.-.G., Hirsch, E., Bartolomei, F, 2019. High-frequency oscillations and spikes running down after SEEG-guided thermocoagulations in the epileptogenic network of periventricular nodular heterotopia. Epilepsy Res. 150, 27–31.
Siegel, J.S., Ramsey, L.E., Snyder, A.Z., Metcalf, N.V., Chacko, R.V., Weinberger, K., Baldassarre, A., Hacker, C.D., Shulman, G.L., Corbetta, M., 2016. Disruptions of network connectivity predict impairment in multiple behavioral domains after stroke. Proc. Natl. Acad. Sci. U.S.A. 113, E4367–E4376.
Silber, M.H., Ancoli-Israel, S., Bonnet, M.H., Chokroverty, S., Grigg-Damberger, M.M., Hirshkowitz, M., Kapen, S., Keenan, S.A., Kryger, M.H., Penzel, T., Pressman, M.R., Iber, C., 2007. The visual scoring of sleep in adults. J. Clin. Sleep. Med. JCSM Off. Publ. Am. Acad. Sleep Med. 3, 121–131.
Silverstein, B.H., Asano, E., Sugiura, A., Sonoda, M., Lee, M.-.H., Jeong, J.-.W., 2020. Dynamic tractography: integrating cortico-cortical evoked potentials and diffusion imaging. Neuroimage 215, 116763.
Steriade, M., Nuñez, A., Amzica, F., 1993. A novel slow (\textless 1Hz) oscillation of neocortical neurons in vivo: depolarizing and hyperpolarizing components. J. Neurosci. Off J. Soc. Neurosci. 13, 3252–3265.
Takeuchi, N., Izumi, S.-.I., 2012. Maladaptive plasticity for motor recovery after stroke: mechanisms and approaches. Neural Plast. 2012, 359728.
Timofeev, I., 2000. Origin of slow cortical oscillations in deafferented cortical slabs. Cereb Cortex 10, 1185–1199.
Tononi G., Cirelli C. 2014. Sleep and the price of plasticity: from synaptic and cellular homeostasis to memory consolidation and integration. Neuron. 2014 January 8; 81(1): 12–34. doi:10.1016/j.neuron.2013.12.025.
Trebaul, L., Deman, P., Tuyisenge, V., Jedynak, M., Hugues, E., Rudrauf, D., Bhattacharjee, M., Tadel, F., Chanteloup-Foret, B., Saubat, C., Reyes Mejia, G.C., Adam, C., Nica, A., Pail, M., Dubeau, F., Rheims, S., Trébuchon, A., Wang, H., Liu, S., Blauwblomme, T., Garcés, M., De Palma, L., Valentin, A., Metsähonkala, E.L., Petrescu, A.M., Landré, E., Szurhaj, W., Hirsch, E., Valton, L., Rocamora, R., Schulze-Bonhage, A., Mindruta, I., Francione, S., Maillard, L., Taussig, D., Kahane, P., David, O, 2018. Probabilistic functional tractography of the human cortex revisited. Neuroimage 181, 414–429.
Tscherpel, C., Dern, S., Hensel, L., Ziemann, U., Fink, G.R., Grefkes, C., 2020. Brain responsivity provides an individual readout for motor recovery after stroke. Brain J. Neurol. 143, 1873–1888.
Usami, K., Matsumoto, R., Kobayashi, K., Hitomi, T., Shimotake, A., Kikuchi, T., Matsuhashi, M., Kunieda, T., Mikuni, N., Miyamoto, S., Fukuyama, H., Takahashi, R., Ikeda, A., 2015. Sleep modulates cortical connectivity and excitability in humans: direct evidence from neural activity induced by single-pulse electrical stimulation. Hum. Brain Mapp. 36, 4714–4729.
Vagnozzi, R., Signoretti, S., Cristofori, L., Alessandrini, F., Floris, R., Isgró, E., Ria, A., Marziale, S., Zoccatelli, G., Tavazzi, B., Del Bolgia, F., Sorge, R., Broglio, S.P., McIntosh, T.K., Lazzarino, G, 2010. Assessment of metabolic brain damage and recovery following mild traumatic brain injury: a multicentre, proton magnetic resonance spectroscopic study in concussed patients. Brain 133, 3232–3242.
Valderrama, M., Crépon, B., Botella-Soler, V., Martinerie, J., Hasboun, D., Alvarado-Rojas, C., Baulac, M., Adam, C., Navarro, V., Le Van Quyen, M., 2012. Human gamma oscillations during slow wave sleep. PLoS ONE 7, 1–14.
Valentín, A., Anderson, M., Alarcón, G., Seoane, J.J.G., Selway, R., Binnie, C.D., Polkey, C.E., 2002. Responses to single pulse electrical stimulation identify epileptogenesis in the human brain in vivo. Brain J. Neurol. 125, 1709–1718.
Volgushev, M., Chauvette, S., Mukovski, M., Timofeev, I., 2006. Precise long-range synchronization of activity and silence in neocortical neurons during slow-wave oscillations [corrected]. J. Neurosci. Off. J. Soc. Neurosci. 26, 5665–5672.
Von Monakov C. 1969. Diaschisis. Brain and Behaviour 1: Mood, States and Mind.
Vyazovskiy, V.V., Olcese, U., Hanlon, E.C., Nir, Y., Cirelli, C., Tononi, G., 2011. Local sleep in awake rats. Nature.
Weliky, M., Kandler, K., Fitzpatrick, D., Katz, L.C., 1995. Patterns of excitation and inhibition evoked by horizontal connections in visual cortex share a common relationship to orientation columns. Neuron 15, 541–552.
Weng, Y., Larivière, S., Caciagli, L., Vos de Wael, R., Rodríguez-Cruces, R., Royer, J., Xu, Q., Bernasconi, N., Bernasconi, A., Thomas Yeo, B.T., Lu, G., Zhang, Z., Bernhardt, B.C, 2020. Macroscale and microcircuit dissociation of focal and generalized human epilepsies. Commun. Biol. 3, 1–11.
Yamakami, I., McIntosh, T.K., 1991. Alterations in regional cerebral blood flow following brain injury in the rat. J. Cereb. Blood Flow Metab Off. J. Int. Soc. Cereb. Blood Flow Metab. 11, 655–660.
Zhang, H., Watrous, A.J., Patel, A., Jacobs, J, 2018. Theta and alpha oscillations are traveling waves in the human neocortex. Neuron 98, 1269–1281 e4.